Journal of Composites and Compounds 5 (2023) 91-101

Available online at www.jourcc.com

Journal homepage: www.JOURCC.com

Journal of Composites and Compounds

A review on bimetallic composites and compounds for solar cell applications

Leila Bazli [a], *Fariborz Sharifianjazi* [a]*, *Amirhossein Esmaeilkhanian* [b], *Maryam Nili-Ahmadabbdi* [c], *Bahman Amini Horri* [d], *Ashish Ravalia* [e], *Safiyeh Mohammadi* [f], *Abdurrahman Yolun* [g], *Kyusun Kim* [h], *Maryam Azimpour* [i], *Shwetha Rani R* [j]

[a] School of Science and Technology, University of Georgia, Tbilisi, Georgia
[b] Department of Materials and Metallurgical Engineering, Amirkabir University of Technology, Tehran, Iran
[c] Materials Engineering Department, Tarbiat Modares University, Tehran, Iran
[d] School of Mechanical Engineering Sciences, University of Surrey, Guildford, Surrey GU2 7XH, UK
[e] Department of Nanoscience and Advanced Materials,Saurashtra University, Rajkot 360005, India
[f] Sciences Faculty, Zanjan University, Zanjan, Iran
[g] Physics Department, Inonu University, 44280 Malatya, Turkey
[h] Department of Nano Engineering, Department of Nano Science and Technology, SKKU Advanced Institute of Nanotechnology(SAINT), Sungkyunkwan University(SKKU), Suwon
[i] Hospital of Shahid Ayatollah Dastgheib, Shiraz University of Medical Science, Shiraz, Iran
[j] Centre for Nano and Material Sciences, Jain University, Jain Global Campus, Kanakapura, Bangalore 562112 Karnataka, India

ABSTRACT

The scientific community has developed new technologies, including solar cells (SCs), to meet global energy demands. SCs convert solar energy into electrical energy, providing renewable, sustainable, and green energy. Despite the availability of PV systems for many years, power generation through SC technology remains costly due to the low conversion efficiency (CE). Their low CE is due to limitations in semiconducting materials. In the present review, the basic mechanism of SC and techniques for modify SC have been discussed. The main focus of this review is to given an overview about the bimetallic materials and their application in SC. Bimetallic materials consist of two metallic components that can be synthesized using different methods. They exhibit exceptional properties, including improved electrical conductivity, tunable electrochemical activity, and high charge capacity compared to monometallic materials, making them promising candidates for use as electrochemical catalysts and photocatalysts. Various types of bimetallic composites and compounds, such as, oxides, phosphide, sulfide and carbon-based bimetallic composites is explained in the context of their compositions, synthesis techniques and their power generation efficiency. In the last portion of review, the importance of bimetallic materials in SC application with their possible promising research direction and challenges are presented.

Peer review under responsibility of UGPH.

ARTICLE INFORMATION

Article history:
Received 29 January 2023
Received in revised form 09 April 2023
Accepted 17 May 2023

Keywords:
Solar cells
Bimetallic
Composites
Compounds
Solar energy

* *Corresponding author: Fariborz Sharifianjazi; E-mail: f.sharifianjazi@ug.edu.ge*

https://doi.org/10.61186/jcc.5.2.4

Table of contents

1. Introduction

The negative impacts of our unsustainable energy practices on society, health, and the environment issues are becoming increasingly apparent, even though global fossil fuel resources are not yet depleted [1-5]. SCs and other renewable energy technologies have been developed as a result of the growing worldwide demand for energy and environmental concerns. To achieve sustainable and enhancement of our living standard, large-scale alternative renewable energy production methods are necessary in the future [6-9]. Without the use of alternate renewable resources, present scenario of increasing electrical energy demands will likely result in significant global warming due to greenhouse gas emissions over the next 50 years. However, advances in science and technology have enabled the production of energy from sustainable sources e.g. solar, biomass, geothermal, wind and energy [10]. Amongst these, solar energy is the most affordable natural resource available today. Utilizing SC technology, which converts sunlight into direct current in the cells, is a very efficient technique to produce power. This technology has been extensively reviewed in the literature [11, 12]. Converting solar energy into electricity was first observed in the 1950s [1]. When two electrodes in a liquid or solid electrolyte are exposed to light, converting solar energy to electricity results in the creation of an electric voltage across the electrodes. The majority of PV devices are fabricated using semiconducting materials with p-n junctions, commonly known as, SCs. For optimum device performance, it is important to select a semiconductor materials with significant absorption ability of solar spectrum [13]. In the late 1950s, the first PV cells were developed and primarily used to power satellites during the 1960s. PV cells were first developed in the late 1950s and were primarily used for spacecraft in the 1960s. Improvements in performance and manufacturing in the 1970s led to lower costs and increased use in remote terrestrial applications. PV power systems were developed for home and commercial use after the energy crisis [14, 15].

Over the past few decades, the manufacture of PV modules is experiencing rapid growth, and their integration onto buildings and connection to utility networks is increasing [16]. A variety of SC technologies are currently available, including silicon-based, thin film, multijunction, and next-generation SCs. Bimetallic composites and compounds have gained significant attention in recent years [17]. Despite the fact that bimetallic materials are important in SC applications, there is not a comprehensive review on this topic. Due to properties including light absorption, enhanced charge carrier transport and separation, and increased stability in harsh environmental conditions, bimetallic composites have gained considerable attention as potential materials for use in SC applications [18]. The combination of two materials' physical properties in SC applications results in improved electron conductivity and excellent catalytic properties. For instance, bimetallic sulfides demonstrate remarkable activity due to their multiple valence states, leading to more extensive redox reactions [19]. According to the research reported by Sarra Bouazizi et al., a (PSC) perovskite SC made of lead-free inorganic materials can achieve an efficiency of 18.13 percent by carefully controlling a number of factors that affect the performance of each layer. ZnO has been shown to improve electron extraction and consequently performance when used as an electron transport layer [20]. Bimetallic composites, which exhibit great light dispersion and a long-range Localized Surface Plasmon Resonance (LSPR) effect, are interestingly better at absorbing photo-current than mono-metallic ones [21-23]. Research has shown that bimetallic nanomaterials and their nanocomposites are promising candidate for SC

Table 1.
Bimetallic compounds used for solar cells application.

Bimetallic Compound	Type of Solar Cell	Premodified				Modified				Ref.
		PCE %	V_{OC}	J_{OC}	FF%	PCE %	V_{OC}	J_{OC}	FF%	
Ag:Zn	Thin Film OSC	1.9	0.56	7.6	45	3.6	0.55	14.0	47	[51]
AuPt	DSSC	1.1	0.651	16.1	31	3.4	0.654	16.5	31	[52]
Au:Ag	Organic SCs	6.72	0.53	19.64	64.9	7.70	0.542	21.43	66	[53]
Ag:Ca		1.99	0.51	8.7	36.7	3.47	0.55	11.6	52.8	[21]
SnCr	Organic SCs	Not eported	Not eported	Not eported	Not eported	1.46	0.99	2.19	10	[31]
Ag:Au	DSSCs	8.78	0.63	3.49	63	14.75	0.68	6.56	65	[50]
Au:Ag/SiO_2	DSSCs	5.4	0.65	11.3	68	7.56	0.68	15	66	[54]

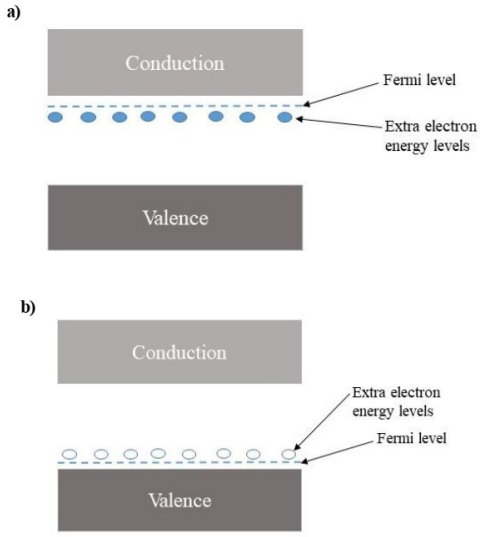

Fig. 1. Energy bands of a) n-type semiconductor b) p-type semiconductor.

applications. Various synthesis and fabrication methods of bimetallic SC have been proposed and studied their SC characteristics.

In this comprehensive review, we delve into the cutting-edge advancements in SC technology, specifically focusing on the utilization of bimetallic materials and their innovative composites. Our primary objective is to explore the intricate working mechanisms and explore novel modification methods employed in the realm of SCs. By categorizing bimetallic materials according to their vast potential in SC applications, we have rigorously assessed the diverse range of SCs that have emerged in this exciting field.

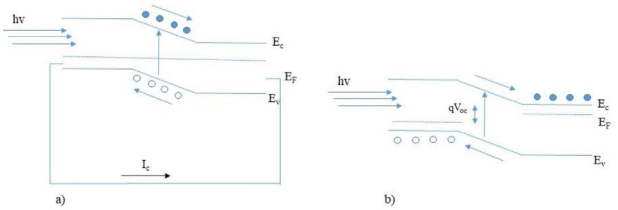

Fig. 2. a) short-circuit b) open-circuit for Solar Cell.

2. Mechanisms in SCs

In a solar energy generation system, a PV cell is the primary component responsible for converting sunlight into electrical energy. It works based on the PV effect and functions as a device with a p-n junction. While the p-type material has holes produced by acceptor impurity atoms, the n-type material has electrons provided by donor impurity atoms. Figure 1(a and b) shows energy band of n-type and p-type semiconductor, respectively.

When sunlight shines on a semiconductor with p-n junction, photons with energies greater than the Eg (band gap) form an e^- (electron) in conduction and h^+ (hole) in valance band. The electric field generated by the ionized impurity atoms in the depletion region causes the h^+ to move toward the p-side while the e^- move toward the n-side. When an external wire is short-circuited, the current flow from n- to p-side is caused by charge separation.

The electron-hole pairs formed within a diffusion length of the depletion region edge contribute to the photo current as a result of the diffusion of additional carriers up to the space charge zone. When the excited p-n junction, is open-circuited, the charge carrier separation

Table 2.
Oxide bimetallic composites used for different type of solar cells.

Bimetallic Compound/Composite	Type of Solar Cell	Premodified				Modified				Ref.
		PCE %	V_{OC}	J_{OC}	FF%	PCE %	V_{OC}	J_{OC}	FF %	
NiO@ZnO	TiO_2-$CsPbI_3$	6.66	15.12	0.73	60	8.73	0.83	16.70	63	[7]
$NiCo_2O_4$@RGO	DSSC	3.03	0.69	8.54	51.42	6.17	0.69	14.92	59.93	[8]
$ZnMoO_4$/3D-AWC						7.65	0.69	16.41	67	
$Cu_3Mo_2O_9$/3D-AWC	DSSC	6.07	0.62	14.86	66	7.33	0.74	15.71	63	[9]
$MnMoO_4$/3D-AWC						6.92	0.65	15.52	68	
Ag:NiO_x@C	Thin-film	2.01	0.55	8.91	42.77	3.47	0.59	13.51	43.46	
Pure Ag:NiO_x	Organic SCs	2.01	0.55	8.91	42.77	4.11	0.55	16.09	46.23	[55]
CuO/CeO_2	ITO	6.48	-	-	-	9.6	-	-	-	[18]
	Si	-	-	-	-	14.52	-	-	-	
CuO@NiO under forward scan		8.58	0.89	18.89	51	10.11	0.91	21.80	51	
CuO@NiO under reveres scan	Perovskite	7.17	0.86	18.52	45	9.49	0.88	20.94	51	[56]
$MnTa_2O_6$@MPC	D35SC	2.93	0.91	6.56	40.40	3.41	0.88	6.85	56.32	[57]
	Y123SC	1.45	0.74	4.27	46.01	1.92	0.75	5.34	47.56	
$CoFe_2O_4$ @C	DSSC	6.36	0.715	13.57	60	7.80	0.737	17.10	62	[58]

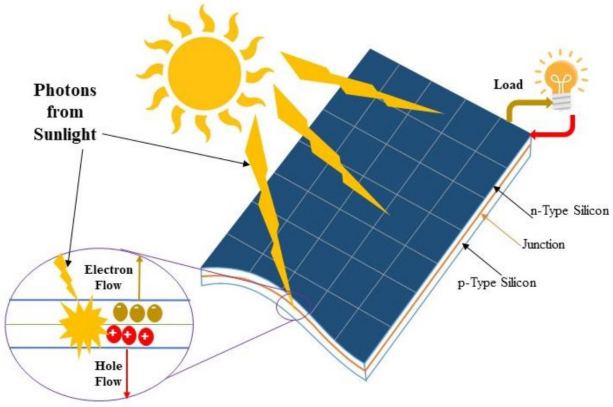

Fig. 3. Schematic of Si-based SC.

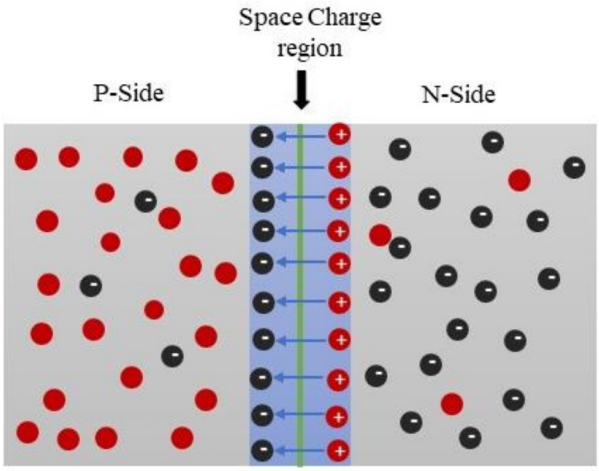

Fig. 4. The p-n junction region and the produced E.

produces the voltage. The p-n junction's energy band diagrams for the open-circuited and short-circuited currents are displayed in Figure 2.

The Isc (current of short circuit), produced when the p- and n-sides are shorted together, is equal to the photo generated current if there is no resistance in the series. Also, a potential is created when the p- and n-sides are not circuited with a wire because electrons migrate toward the n-side and holes toward the p-side. This developed potential is known as the Voc (open-circuit voltage).

The current voltage of the p-n junction that is illuminated is given by equation (1) assuming the SC's area is unity.

$$I = I_0(e^{qV/nKT} - 1) - I_{sc} \quad (1)$$

Although I = 0 is used to obtain the open-circuited, the voltage can be obtained by:

$$V_{oc} = \frac{nkT}{q} In(\frac{I_{sc}}{I_0} + 1) \quad (2)$$

The fill factor is the ration of $V_m.I_m$ to I_{sc} .V_{oc} which V_m and I_m are voltage in SCs for maximum output.

$$FF = \frac{V_m I_m}{V_{Oc} I_{sc}} \quad (3)$$

The ratio of the greatest electric output power produced to the total power of the incident light Pin is known as the CE (conversion efficiency) of the SCs, or η.

$$\eta = \frac{V_m I_m}{P_{in}} = \frac{V_{oc} I_{sc} FF}{P_{in}} \quad (4)$$

Under normal test settings, IPD (incident power density) of 1000 W/m^2, the T of 25° C, and an air mass (AM) 1.5 spectrum, the PV parameters are tested. It is required to maximize PV parameters, e.g. FF, Isc, and Voc, in order to increase efficiency [24].

The PV effect involves three essential steps that contribute to the cell's operation [25, 26].

1. When a p-n junction semiconductor observes photons, electron-hole pairs are produced. This phenomenon is known as the PV effect. A hole results from an electron moving from the valence band (E_v) to the conduction band (E_c) when a photon with enough energy (greater than E_g) absorbed. The photon's surplus energy (h-h_0) gives the electron or hole more kinetic energy. The symbol "h00," which stands for the energy gap or work function of the semiconductor, indicates the minimal amount of energy or work function needed to create an electron-hole pair. Any energy exceeding this minimum requirement is converted into heat within the semiconductor material [26, 27].
2. The next stage of the PV effect consists of separating the charge carriers generated by light. The electrons can escape over the specific n-region and go through the circuit before recombining with the holes, whereas the holes can flow through the designated p-region and away from the junction once in an external solar circuit.
3. The final stage of the PV effect involves utilizing the separated electrons to produce an electric current. The electrons

Table 3.
Sulfide Bimetallic composites composites used for different type of SCs.

Bimetallic Compound/Composite	Type of Solar Cell	Premodified				Modified				Ref.
		PCE %	V_{OC}	J_{OC}	FF%	PCE %	V_{OC}	J_{OC}	FF%	
Co_9S_8/NC@$FeCoS_2$CNC	DSSC	5.24	0.715	13.01	68.5	7.07	0.724	13.75	0.71	[66]
$NiCo_2S_4$	Thin film SCs	7.60	0.70	16.70	0.65	8.10	0.69	18.43	64	[67]
Ni_3S_4/CoS_2	DSSC	5.8	0.624	12.31	61	10.1	0.842	18.12	83	[68]
$NiCo_2S_4$/TiO_2	DSSC	Not reported	Not reported	Not reported	Not reported	8.29%	0.828	14.39	69.52	[64]
Co@MoS_2	DSSC	6.94	0.74	14.29	66	8.99	0.75	17.64	68	[69]
$NiCo_2S_4$	CdS/CdSe quantum-dot-sensitized SC	1.3	0.489	11.76	22.56	3.14	0.489	16.68	38.52	[70]
NiS_2/CoS_2-0.1	Thin film SCs	6.83	0.71	15.26	63	8.22	0.72	17.45	65	[71]
Co_8FeS_8/N-C	DSSC	7.17	0.72	16.47	60	8.06	0.75	18.19	58	[65]
$CuSbS_2$	DSSC	Not reported	Not reported	Not reported	Not reported	2.60%	0.709	6.765	54.4	[72]

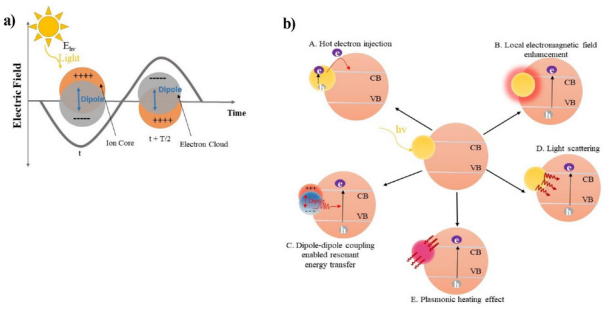

Fig. 5. a) LSPR mechanism, b) Diagrams of Different Mechanisms for LSPR-Enhanced Photoactivity of Semiconductors.

are passed through a designated circuit; after which they will eventually combine with the holes. To ensure an efficient flow of electrons, the n-type material is designed to be thinner than the p-type material. This enables the electrons to move quickly through the circuit and produce current before joining the holes. Additionally, the n-layer is coated with an anti-reflective substance to lessen surface reflection and improve light transmission to the semiconductor material. This improves how well light is transmitted to the semiconductor material [25].

As per the above discussed mechanisms of PV effect, a SC is a special kind of semiconductor diode designed to harness the energy of sunshine. Single crystal semiconductor, e.g. silicon, doped with pentavalent and trivalent impurities on opposite sides, respectively, to create the n and p type semiconductor. Doping generates high number of more mobile charge carriers, also known as, majority carriers, in both regions. An area of positively charged donor atoms forms at the p-n interface, which is close to the n-zone, where the p and n-type semiconductors come into contact. The reason for this is the diffusion of electrons from the n-region into the p-region. A net of acceptor atoms that are negatively charged and act as holes move from the p-region to the n-region and then enter the p-zone in the vicinity of the p-n junction. The movement of the holes can be used to detect the mobility of the valence electrons. The formation of the diffusion current, also known as I_{diff}, and a region of depleted charge carriers known as the space charge region (or depletion region) are both results of the diffusion of holes and electrons [28]. Figure 3 shows schematic of Schematic of Si-based SC.

Under equilibrium conditions, the motion of charge carriers in a semiconductor results in two types of current: diffusion current (I_{diff}) caused by the concentration gradient and drift current caused by the electric field at the junction [29]. The electron diffusion current, denoted as $I_{n\text{-}diff}$, can be determined using the equation:

$$I_{n-diff} = eDn.\left(\frac{dn}{dx}\right) \quad (5)$$

where D_n is the diffusion coefficient of electrons. The hole I_{diff} density is similarly given by

$$I_{p-diff} = -eDp.\ (dp/dx) \quad (6)$$

where D_p is the diffusion coefficient of holes.

The hole diffusion distance to the variations in particle density to the change in their diffusion length and ratios of the variations in electron is represented by *dp/dx* and *dn/dx*, respectively. The built-in electric field in the depletion region generates a current opposite to the diffusion current, known as *'I_{drift}'* [30].

The drift current of electrons, *'$I_{n\text{-}drift}$,'* is expressed as

$$I_{n-drift} = en\mu_n E = envdn \quad (7)$$

where *'μn'* denotes the mobility of electrons, *'E'* denotes the E in the depletion region, and *'udn'* denotes the drift velocity of electrons. The current due to the drift of holes, '*$I_{p\text{-}drift}$,'* can be similarly expressed.

$$I_{p-drift} = ep\mu_p E = epudp \quad (8)$$

'μ_p' is the hole's mobility and '*udp*' is the average drift velocity of holes. The net 'I_{drift}' due to drift of holes and electrons is as follows:

$$I_{drift} = e\ (\mu_n n + \mu_p p)\ E \quad (9)$$

The above equation can be written as:

$$I_{drift} = e(\mu_n n + \mu_p p)E = \sigma E \quad (10)$$

$$\sigma = e(\mu_n n + \mu_p p) \quad (11)$$

The I_{diff} ($I_{n\text{-}diff}$ for electrons and $I_{p\text{-}diff}$ for holes) is proportional to the gradient of particles' densities with respect to the diffusion distance of electrons and holes. On the other hand, the built-in E generates the drift current ($I_{n\text{-}drift}$ and $I_{p\text{-}drift}$), which is opposite to the I_{diff}. Electron mobility (*n*), the electric field in the depletion area (*E*), and drift velocity together produces the drift current of electrons ($I_{n\text{-}drift}$) (*udn*). Similarly, the average drift velocity of holes and their mobility *(p)* are the two factors that determine the drift current of holes ($I_{p\text{-}drift}$) (*udp*). The equation *e(n n + p p)E* or *sE*, where *s = e(n n + p p)*, may be used to calculate the total drift current (I_{drift}), which is the sum of the drift currents of electrons and holes.

The electronic semiconductor's conductivity (*s*, given in W/cm) determines the motion of electrons or holes through the material when sub-

Table 4.
Carbon-Bimetallic composites used for solar cell applications.

Bimetallic Compound/ Composite	Type of Solar Cell	Premodified PCE %	Premodified Voc	Premodified Jsc	Premodified FF %	Modified PCE %	Modified Voc	Modified Jsc	Modified FF %	Ref.
Mn/Co-NGC*	DSSC	5.9	-	-	-	8.05	-	-	-	[77]
Pt-Ni/rGO*	DSSC	3.30	0.819	20.75	19	6.14	0.749	14.08	58	[81]
NTiBi/rGO	DSSC	4.26	0.48	13.83	63.58	7.20	0.63	14.52	78.86	[82]
Co-TiC/Carbon NanoFiber	DSSC	Not Reported	Not Reported	Not Reported	Not Reported	3.87	0.758	9.98	50.7	[29]
WMo/rGo	DSSC	Not Reported	Not Reported	Not Reported	Not Reported	4.28	0.694	8.951	69	[30]
Ni-Co/rGo	DSSC	0.46%	0.67	0.85	32	3.10%	0.70	9.1	48	[83]
Ni-Co/CNFs	DSSC	5.5%	0.74	7.30	58	4.57%	0.73	9.78	64	[84]
FeNi@N-G	DSSC	Not reported	Not reported	Not reported	Not reported	4.12%	0.73	8.96	63	[85]
$CoSe_2$/N-C@CC*	DSSC	5.22%	0.685	11.97	63	8.09%	0.73	16.39	0.70	[79]
CoSe@N-G*	DSSC	6.62%	0.731	13.58	66.2	7.65%	0.745	15.40	66.66	[80]

* N-coordinated Graphitic Carbon
* rGO: Reduce graphene
*N-C@CC: N-doped carbon nanocage@ Carbon Cloth
* N-G: N doped Geraphene

jected to an electric field. In nondegenerate semiconductors, the equilibrium state is reached when the drift current (I_{drift}) and diffusion current (I_{diff}) are balanced, resulting in no net currents in the depletion region. This equilibrium state is described by the Einstein relation: $D\,\mu = kT/e$. The particle mobility (μ) indicates an electron or a hole motion under an E, while the D, known as the particle diffusion coefficient, indicates how well the particles motion is due to concentration gradients within the semiconductor [31, 32].

2.1. The Evolution of SCs

2.1.1. First generation of PV

The original generation of SCs, which are Si-based SCs, are the oldest and most commonly used. These SCs, which can be either Monocrystalline, Poly crystalline and Amorphous crystalline silicon, are also referred to as conventional, traditional, or wafer-based cells. Bell Laboratory made the initial discovery of silicon SCs in 1954, with a PCE (power convertion efficiency) of 6%. Considering single-cell PV modules, silicon SCs are among the most effective systems due to their accessibility and availability on the surface of the globe. Due to the incorporation of these materials into a PV device with a 1.1 eV band gap, which is ideally suited for PV applications. The efficiency of silicon SCs is currently 26.6%. The Czochralski process is used to create single crystal wafers in silicon devices, and it accounts for around 30% of the market. Compared to polycrystalline Si and amorphous Si solar panels, single crystalline silicon is purer and more prevalent. Due to the way, silicon is arranged structurally, polycrystalline Si is less expensive than monocrystalline Si. The poly c-Si SC with the highest documented PCE is 21%. However, the expense of manufacturing single-crystalline Si SCs prevents the idea of low-cost manufacture [33, 34].

2.1.2. Second generation of PV

Second generation thin film SCs (TFOSC), which have attracted interest from the scientific community, were created as an alternative to silicon SCs by depositing multi or one semiconductors thin layer on a substrate such as glass, plastic, or metal. Because semiconductors have a high optical absorption coefficient ($>10^4$ cm^{-1}), less film thickness is needed. Despite major advancements in recent years, thin film SCs have been less expensive but less effective than traditional silicon SCs. The difficulty in controlling the stoichiometry, complex deposition process, and existence of structural flaws are the key points of contention in these second generation SCs [33].

2.1.3. Third generation of PV

Third generation SCs are a type of SCs that evolved as a result of the first generation's SCs being more expansive, the second generation's SCs having a limited supply of raw materials, and the second generation's SCs' poisonous effects. Because third-generation SCs don't rely on p-n junction, they are fundamentally distinct from the other generations of SCs. Perovskite SCs (PSCs), quantum dot SCs (QDSCs), dye-sensitized SCs (DSSCs), and organic SCs (OSCs), which have met the criterion of cheap production costs, are examples of third generation SCs, sometimes referred to as emerging PVs. Due to their unique qualities, including easy manufacturing processes, affordability, environmental friendliness, transparency, good plasticity, good conductivity, and high efficiency, DSSCs offer advantages over other photo voltaic devices. The difference in energy between the solar photon and semiconductor's Eg, while radiative recombination in the SCs acting as the lone loss process, determines the theoretical efficiency of a SCs. Photo-excitation can be caused by any photon with energy higher than or equal to the Eg and photon with energy below can't cause photo excitation. The "tandem cell" or "multi-junction" strategy, which involves putting thin layers of material with different band gaps on top of one another, is how third-generation cells are created in order to solve these issues [33, 35].

2.2. Modification of SCs

As mentioned before, the objective of modifying SCs is to enhance their ability to convert sunlight into electrical energy, which is referred to as PCE. While based on Shockley Queisser (SQ) Efficiency the maximum theoretical PCE for a single-junction SC is approximately 33.7%. The SQ limit only permits radiative recombination in the extreme, where a single SC transforms 30% of solar energy into electrical energy at one sun irradiance (1000 W/m^2). The SQ limit, which only applies to cells with a single p-n junction, can be exceeded by cells with several layers [36, 37].

Various methods such as doping, defect passivation, and interface engineering have been proposed and understood to improve this value [38]. PCE represents the proportion of sunlight energy that can be converted into electrical energy via PVs. High PCE SCs possess several advantages, including a tunable band gap, strong absorption coefficients, lengthy exciton diffusion lengths, exceptional carrier mobility, and low production costs. They have the potential to surpass other types of SCs and have benefits over inorganic SCs such as shorter energy payback times and lower costs. Moreover, they play a crucial role in large-scale electricity generation [39].

Doping is a widely studied method for modifying photoanodes in SCs. Researchers and scientists have performed various studies to investigate the impacts of element doping on SC efficiency [1, 2, 40]. Modifying the E_g and shifting the optical absorption edge to higher wavelengths [3], controlling morphology [4], can lead to improvements in SC performance observed in literature. In the case of new generation oxide thin film based SC, e.g., ZnO based SC, the efficiency of a cell is affected by the thickness of the ZnO nanoparticle layer. The EQE (External Quantum Efficiency) increases as the layer thickens, reaching up to 80.29 nm. After which starts to decreases due to the presence of various defects. These defects increase carrier recombination, which reduces EQE by lowering collection efficiency [6]. Pirashanthan et al. observed the impact of Lithium-doped TiO_2 based hybrid SCs. They have observed that using Lithium-doped P3HT instead of pristine P3HT increased cell efficiency by almost four times. The enhancement was attributed to the superior light harvesting and charge transport properties of the P_3HT polymer which doped with Lithium, which resulted in a high Isc of over 13 mA/cm^2 [7]. Gupta et al. have investigated the use of Cu/S @TiO_2 NP as a photoanode in DSSCs. Cu/S co-doping changed the optical properties of TiO_2, which lead to increase the absorption in the VLR and resulting in a red shift in Eg. With a much higher Isc of 22.05 mA/cm^2, the DSSC made with TiO_2/0.3 at% Cu and 0.05 at% S displayed the greatest PCE of 10.44%. [3]. Fei Zhao et al., employed Li: TiO_2 (Li-doped TiO_2) as a new electron-transporting layer for $CsPbIBr_2$ Perovskite SCs (PSC). Utilizing the Li: TiO_2 boosted the TiO_2 film's crystallinity, reduced dark current, and reduced charge recombination in the $CsPbIBr_2$ PSC, increasing efficiency from 6.63% to 8.09% [8]. A study of Al and Cu doping on ZnO revealed that doping induced improvement in conductivity and mobility in Cu–ZnO and Al–ZnO films compared to pure films. In the visible spectrum, the ZnO doped with Al and Cu films had a low resistance and an average transmittance of about 80%. Also, the efficiencies for Al-ZnO- and Cu-ZnO-based SCs were reported at 0.492% and 0.559%, respectively [9]. Cobalt-doped NiO_x acted as a hole transport layer in PSC, and annealing it with NIR (near infrared ray) methods resulted in an improvment in PCE 15.99% to 17.77%. This was due to well-matched work function, leading to less charge accumulation, efficient hole extraction, and reduced Voc loss, and improvement in hole mobility, which reduced interface resistance [40].

Interface engineering is an important method, which can signifi-

cantly improve the effectiveness of SCs by optimizing the interfaces between different materials. It involves adjusting the interface between different materials within a SC to enhance its functionality. This process can have a noteworthy impact on the efficiency of SCs, as it can also impact on several properties, which are essential for their operation. Many methods, in which, interface engineering can improve the efficiency of SCs include reducing recombination, increasing charge carrier separation, and enhancing the transmission of light.

One approach is to increase the efficiency of SCs by modifying the interface between the semiconductor and the metal contact within the SC. This technique can help to reduce the rate at which electrons and holes recombine and minimize the amount of energy lost as heat, resulting in higher efficiency. Another way to enhance efficiency is by engineering the interface between different materials within the SC, produces a built-in electric field that separates the positively and negatively charged carriers generated by the absorption of light. This can increase the number of charge carriers collected by the electrodes, leading to improvement in efficiency.

Changing the contact between the semiconductor and the anti-reflective coating in the SCs to increase light transmission into the cell is another method to increase efficiency. This method can improve the efficiency of the cell by allowing more photons to be absorbed by the semiconductor. In conclusion, interface engineering is a crucial approach to improve the effectiveness of SCs. By optimizing the interfaces between different materials, higher efficiency can be achieved in converting solar radiation into electrical energy, leading to the development of renewable and clean energy resources [41, 42].

To enhance the functionality of perovskite SCs, other studies have also been carried out. Huan Bi et al. used a multi-active site Lewis-based molecule called emtricitabine to enhance the PCE from 20.83% to 22.24%. Low defect density in the perovskite thin film and greater interfacial hole extraction because of a better energy match are the reasons for the increased efficiency [43]. Muhammad Ashraf et al. studied the impact of polymeric carbon nitride (C_3N_3, C_3N_5, C_3N) on the performance of PSC. They found that charge carrier recombination could be reduced by the intrinsic electric field band alignments in C3N5. Additionally, the redox reaction between Ni^{3+} and organic cations was suppressed [44]. Creatine was used by Guan-Woo Kim et al. on perovskite thin films as a surface passivation layer and additive to reach a CE of 22.6%. The creatine layer not only protected the perovskite thin film but also improved its operational stability in humid conditions (50% relative humidity) and high thermal (85 °C) [45]. In a different work, iethyldithiocarbamic acid diethylamine (DADA), an organic amine molecule, was used to passivate the ionic defects on the surface of the inorganic perovskite film CsPbIxBr3-xThe device's ambient stability was much enhanced by the DADA passivation, and over the course of 800 hours in an environment with a relative humidity of 30–40%, the Power Conversion Efficiency remained close to 90%. Under 100 mW cm^2 light, this combination increased the SC efficiency from 18.56% to 20.06% [46]. Finally, Katta et al. engineered a passivation layer of neodymium and erbium into the TiO_2 for DSSCs application. In a photoelectrochemical device, the optimized codoped TiO_2 photoanode produced a greater photocurrent density (Jph), measuring 16 A cm^2, than the device with pristine TiO_2 (Jph: 7 A cm^2). [47].

3. Bimetallic materials for SC applications

Additionally, the integration led to improved better simulated photocurrent density of 22.30 mA cm^2 [48]. According to Yaoming Xiao et al., Pt-Ni bimetallic nanocrystals showed excellent electrocatalytic activity to I3- in DSSCs, and the DSSC built with Pt3Ni displayed a higher PV conversion of 7.75% than the DSSC built with Pt CE (7.26%) [5]. NPs of bimetallic are interestingly well-suited to absorbing photo-current rather than mono-metallic ones since the former exhibit strong light dispersion and a long-range LSPR impact. In addition, NPs of bimetallic have the potential to create a strong local electromagnetic field (EMF) that will cause increase trapping, light scattering, and aid in the dissociation of exactions, as well as the LSPR effect in the layer of solar absorber [21]. In reaction to an external EM (Electromagnetic Field) of incoming light, the delocalized electrons in metal oscillate coherently collectively according to SPR. Surface Plasmon oscillations of free electrons are constrained by the geometric boundaries of metal nanostructures. SPR for metal nanostructures is hence frequently referred to as localized SPR (LSPR) [22]. Figure 3, a shows the SPR mechanism. In general, the incident EM can eject hot electrons, or free electrons from metal, into the semiconductor. By directly contacting the Schottky barrier created by the metal nanocrystals and semiconductors, the hot electron with a sufficient jerk can overcome it. As a result, it has the ability to be injected into the semiconductor's CB (Fig 3 b,E). Additionally, the input photon's electric field component can create an energy-storing dipole moment in the metal by charge polarization of surface. By oscillating at the frequency of the input photons, this induce dipole moment causes resonance absorption via Surface Plasmon Resonance (SPR) (Fig 3 b,A). At the metal interfaces, the dipole moment of formed metal can bring about induction a second dipole, resulting in the so-called dipole-dipole interaction between the NPs of metals and nearby semiconductors. (Fig 3 b,B). When the LSPR decays, phonon-electron relaxation of the energy stored in the process results in a photo-thermal reaction, where the obtained mobile carriers' energy is converted to heat. This impact may manifest during the LSPR's non-radiative decay phase. (Fig 3 b,D). It's interesting to note that the pulsating plasma finally demoted by transferring heat energy to the nearby molecules or compounds. (Fig 3 b,D). Last but not least, the interaction of EM with the surface electron plasma of metal can produce a localized electromagnetic field around the metal which can result in near-field scattering. (Fig 3 b,C). All of these mechanisms would help to increase the amount of photons captured and the amount of photocurrent captured through exciton dissociation mechanisms [21].

Abdallah Y. A. Ahmed et all., reported an enhancement of photocurrent for through Silver doped magnesium bimetallic in a TFOSC's photoactive layer. In comparison to the reference cell, the maximum PCE of 4.11% was attained at a 1.5 wt% doping level. The performance enhancement of PCE represents an improvement of 79% in comparison to undoped SCs. The emergence of the LSPR, that's beneficial for enhancing the charge transport processes and optical absorption in SCs, was credited with producing this result [23]. The PCE of the plasmonic Quantum dot SC with the TiO_2/CdS/AuAg (3:1) film was 4.94%, that is 52% bigger than the PCE of the non-plasmonic cell. Upon illumination, electrons in the TiO_2/CdS film are promoted from the CdS VB to the CdS CB. Then, these electrons cascade to the TiO_2 CB and are then sent from TiO_2 to the FTO or current collector. This electron transfer method is favored by the energy level offsets of FTO, TiO_2, and CdS. However, when the TiO_2/CdS/AuAg (3:1) film is exposed to radiation, in addition to the intrinsic electron and holes pairs production in CdS, the near-field plasmonic impact of AuAg alloy leads the production of additional electron and holes pairs in CdS, and the far-field impact causes the mid-gap states in CdS to get populated. As a result, the photocurrents are enhanced not The Fermi energy of pure AuAg (3:1) alloy NPs is 4.65 eV, while the EF' for the TiO_2/CdS/AuAg (3:1) film is 4.43 eV, that is upshifted by 0.22 eV. Since the upshifted Fermi level is above the work function of the FTO, every possible thermodynamically permitted electron transfer from EF' to the FTO is also possible [49]. The implementation of Au-Ag implantation by Navdeep Kaur and co-authors caused to an improvement in the CE and reduced back recombination of TiO_2 sensitizers. The results of DSSCs showed a remarkable 87.97% improvement in PCE. The implantation of bimetallic Ag and Au will enhance TiO_2's capacity

for light absorption and limit back recombination processes, which will enhance electron transport and enhance the PV performance of DSSCs. Huge photo-generated electrons are generated from excited molecules of N719 dye, especially those that are present close to Ag and Au when light strikes the photoanode of DSSCs. Due to their capacity for charge storage, Au and Ag rapidly accumulate photo-generated electrons; this causes the photoanode's Fermi energy level (EF) to shift upward, which effectively transports the accumulated electrons to the CBof TiO_2. Additionally, the plasmonically excited Ag and Au generate electrons that fill the TiO_2's trap levels, that decreases the photo-generated electrons's random charge distribution in TiO_2 and prevents recombination processes at the photoanode/electrolyte interface. Additionally, via the TiO_2 compact layer deposited FTO and collection at Pt CE30, photogenerated electrons from the TiO_2 C.B. are delivered to the external circuit. Thus, by lengthening the electron lifespan and the transport channel, Au and Ag in TiO_2 would effectively improve the charge transportation processes across the DSSC. The underlying investigations have thoroughly supported the above-mentioned notion, which shows superior charge transportation procedures and increased light harvesting ability in bimetallic Ag and Au implanted photoanode-based DSSCs [50].

Various bimetallic compound used for SC application and their first and modified efficiency with their respective references are tabulated in table 1.

In the next section, studies on different types of bimetallic materials, from bimetallic composites to Oxide, Phosphide, Sulfide, and Carbon-Bimetallic composites have been discussed in the context of their SC application.

3.2.1 Oxide Bimetallic composites

Bimetallic oxide composites and compounds have become increasingly popular in the field of SC applications, according to recent research. Binary metal oxide composites are known to possess superior properties compared to their individual constituents. Wafaa M. Salih investigated on the effect of combining CuO and CeO_2 on SC efficiency. The study found that the efficiency of ITO substrate SCs increased to 9.6%, and single crystal solar Si cells increased to 14.52%. The improved efficiency was attributed to the increased concentration of CuO, which has a smaller particle size than CeO_2 and results in a larger surface area to volume ratio [18]. In a recent study, Sakthi Velu Kuppu and colleagues modified the TiO_2-$CsPbI_3$ photoanode by incorporating NiO@ZnO. The UV-Vis spectra analysis revealed that NiO@ZnO was more effective than NiO/ZnO in modifying TiO_2-$CsPbI_3$. The implementation of NiO@ZnO resulted in a higher efficiency of 8.73% for the modified TiO_2-$CsPbI_3$, as compared to the individual use of NiO or ZnO [7]. In a recent study, Sakthi Velu Kuppu and co-worker have shown modified the TiO_2-$CsPbI_3$ photoanode by incorporating NiO@ZnO. The UV-Vis spectra analysis revealed that NiO@ZnO was more effective than NiO/ZnO in modifying TiO_2-$CsPbI_3$. The implementation of NiO@ZnO resulted in a higher efficiency of 8.73% for the modified TiO_2-$CsPbI_3$, as compared to the individual use of NiO or ZnO [7]. Researchers have recently investigated the effects of Ag:NiO_x composites on organic thin film SCs. The study involved the synthesis of two types of composites, namely green Ag:NiO_x with carbon traces and pure particle black Ag:NiO_x. The results showed that adding 1 wt% of Ag:NiO_x resulted in a PCE of 5.1% and 4.95% for black and green composites, respectively. However, adding more than 1 wt% of Ag:NiO_x led to a decrease in the efficiency of the absorber layers [55]. Feng Han conducted a comparative study of $ZnMoO_4$, $Cu_3Mo_2O_9$, and $MnMoO_4$ as 3D network structures on carbon derived from aloe waste. The work function and energy level of the three compounds were measured, with $ZnMoO_4$, $Cu_3Mo_2O_9$, and $MnMoO_4$ showing values of 3.55, 4.86, and 3.62 eV, and 1.25 eV, 0.06, and 1.18 eV, respectively. This suggests that $ZnMoO_4$ is expected to exhibit higher efficiency compared to the other two compounds [9]. Different oxide bimetallic composites used for SC application and their first and modified efficiency with their respective references are tabulated in table 2.

3.2.2 Phosphide Bimetallic composites

Yi Di and co-worker have studied the potential use of phosphide bimetallic composites as a counter electrodes (CEs) for DSSCs. The composites consist of a NiCoP NPs and NiCoP/carbon nanotubes (CNTs). The researchers investigated the performance of these composites and found that the optimal composite CE (NiCoP-CNTs-3) had a PCE of 7.24%, which was higher than the single CNTs electrode (6.05%) or NiCoP (4.71%). The PCE of NiCoP-CNTs-3 was also comparable to that of the standard Pt CE (7.12%) under the same conditions [59].

Lijun and colleagues synthesized Nickel Cobalt Phosphide as a CE for DSSCs using a phosphating reaction. Through electrochemical investigations, they have observed that the CE of NiCoP (8.01%) was superior to that of NiP (3.73%) and CoP (2.80%). The researchers attribute the higher CE of NiCoP to the adjustment of valence electrons and the provision of two electron-donating active sites due to the introduction of two metals [60]. A magnetic CoP@FeP_4 thin film was developed on carbon paper (CP) via a two-step process and evaluated as a CE for DSSCs. The morphology of CoP@FeP_4@CP, which resembles a silkworm, offers several benefits, including improved catalytic performance for the reaction of interface, better connection among the electrolyte and electrode material, and faster electron transmission. In DSSCs, CoP@FeP_4@CP CE achieved a high PCE of 9.88%, that surpassed that of Pt (7.49%) and CoP@CP (8.73%) CEs [61].

3.2.3 Sulfide Bimetallic composites

Transition metal sulfides are known for their exceptional catalytic characteristic in the reduction of triiodide. Bimetallic sulfides, in particular, exhibit synergistic effects among the two metals they contain. The lower band gap energy of these materials can help overcome kinetic barriers and facilitate ion transport and electron transfer. Additionally, the presence of a second metal can lead to an energy shift of the S and Co atoms, shifting the center of the d-band with respect to the Fermi level. This can help reduce the chemical interactionamong the the intermediate and catalyst surface during catalysis, thereby increasing both the catalytic activity and the intrinsic conductivity for certain processes [62]. Materials of this kind are significant for their applications in SCs. Xing Qian and co-worker have developed a catalyst for I3- in dye-sensitized SCs' reduction by synthesizing a double-shelled structure of CoMoSx@Ni-CoMoSx. This composite exhibited a PCE of 9.30%, responsible to the availability of more active sites and increased contact area for the electrolyte [63]. Qin Wu and colleagues fabricated a counter electrode using Co_9S_8/NC@$FeCoS_2$CNC composites, which achieved a CE of 7.07% [43]. A CE consisting of $NiCo_2S_4$/TiO_2 with high reflectance was prepared on TiO_2 coated by FTO glass via a single step hydrothermal method. The mirror-like structure of the CE enhances its electrocatalytic activity and light reflectivity. This results in a big PCE of 8.29% in the DSSC [64]. Co8FeS_8/N-C DNCs have been developed as a cost-effective alternative to platinum CE for DSSCs. They have demonstrated a notable PCE of 8.06%. The electrochemical analysis highlights the excellent electrocatalytic activity of Co_8FeS_8 DNCs for triiodide reduction, with minor peak-to-peak separation and electron transfer impedance compared to both platinum and monometallic sulfide Co_9S_8/N-C counter electrodes [65]. Different sulfied bimetallic composites used for SC application and their first and modified efficiency with their respective references are tabulated in table 3.

3.2.4 Carbon-Bimetallic composites

Carbon materials have been identified as promising electrode materials in new energy devices namely, fuel cells, supercapacitors, and SCs [73, 74]. This is because of their unique advantages such as high surface area, low cost, and excellent electrical conductivity [75]. However, the sp2 or sp3 hybridization in pristine carbon limits the available active sites and results in low catalytic activity. To overcome this limitation, various modification methods in synthesis have been explored to increase the activity of carbon-based catalysts [76]. As reported by Asim Arshad and colleagues, a modified graphitic carbon material was synthesized by incorporating N-coordination and Mn/Co via pyrolysis. The resulting Mn/Co-NGC (N-coordinated bimetal doped graphitic carbon) composite showed a PCE of 8.05%, which outperformed the PCEs of Co-NGC, NGC, and Mn-NGC (6.6%, 5.9% , and 7.1%, respectively). The enhanced electrocatalytic activity of Mn/Co-NGC for the reduction reaction of triiodide in SCs was attributed to its superior PCE and short-circuit current density (Jsc) values [77]. The current study involved the incorporation of active CuNi bimetallic NPs inside carbon nanofibers, and subsequent testing of the synthesized nanofibers-based DSSC. Results investigated a PCE of 3.5%, with a Isc of 7.67 mA/cm^2 and an Voc of 0.70 V [78]. The photocathode of a DSSC was prepared using $CoSe_2$/N-C supported on carbon cloth, and it exhibited excellent long-term stability and a high PV efficiency of 8.40%, surpassing that of Pt. The superior performance is attributed to several factors, such as the high $CoSe_2$'s catalytic activity, efficient mass transfer facilitated by the porous 3D structure, and excellent electron transport resulting from the strong interaction among $CoSe_2$ and the highly conductive carbon cloth [79]. CoSe@N-G composites were recently synthesized as a potential replacement for Pt electrodes in DSSCs. The composite demonstrated a higher CE of 7.65%, compared to the Pt electrode's 7.19%. The addition of more N-doped graphene (N-G) resulted in further improvement in CE. This high PCE% is responsible for the even distribution of $CoSe_2$ and the excellent conductivity of N-G [80]. Various carbon- bimetallic composites used for SC application and their first and modified efficiency with their respective references are tabulated in table 4.

4. Conclusions and future insights

In conclusion, bimetallic composites and compounds have emerged as promising materials for solar cell applications. The electronic multifunctionality, heterogeneity, and specific site response offered by bimetallic structures make them attractive for improving power conversion efficiency. In our study, we focused on oxide, phosphide, sulfide, and carbon-bimetallic composites individually. While oxide, sulfide, and carbon-bimetallic composites have been extensively studied, phosphide bimetallics still hold untapped potential and present an intriguing avenue for future research. Exploring the capabilities of mono-metallic phosphide elements in SC applications could yield valuable insights and contribute to further advancements in SC technology. Ultimately, harnessing the unique properties of bimetallic materials has the potential to revolutionize the solar energy field, facilitating the development of more efficient and sustainable SCs.

Acknowledgments

The authors received no financial support for the research, author-ship and/or publication of this article.

Conflict of interest

The authors declare that there is no conflict of interest.

REFERENCES

[1] J.-S. Kim, V.-D. Dao, L.L. Larina, H.-S. Choi, Optimum alloying of bimetallic PtAu nanoparticles used as an efficient and robust counter electrode material of dye-sensitized solar cells, Journal of Alloys and Compounds 682 (2016) 706-712.
[2] R. Selvapriya, J. Vinodhini, T. Abhijith, V. Sasirekha, V. Ragavendran, J.M. Pearce, J. Mayandi, Fabrication of bimetallic inlaid working electrode for highly efficient dye sensitized solar cells, Journal of Alloys and Compounds 939 (2023) 168634.
[3] M. Tang, B. Sun, D. Zhou, Z. Gu, K. Chen, J. Guo, L. Feng, Y. Zhou, Broadband plasmonic Cu-Au bimetallic nanoparticles for organic bulk heterojunction solar cells, Organic Electronics 38 (2016) 213-221.
[4] E.A.A. Arbab, G.T. Mola, Metals decorated nanocomposite assisted charge transport in polymer solar cell, Materials Science in Semiconductor Processing 91 (2019) 1-8.
[5] Y. Xiao, G. Han, Y. Li, M. Li, J.-Y. Lin, Three-dimensional hollow platinum–nickel bimetallic nanoframes for use in dye-sensitized solar cells, Journal of Power Sources 278 (2015) 149-155.
[6] N. Raleie, V.S. John-Denk, N.W. Hlongwa, S.F. Douman, E.I. Iwuoha, Photoelectrochemistry of Poly-3-hexylthiophene and Stannum Chromium Bimetallic Nanoparticle Heterojunction Blend, Electroanalysis 32(12) (2020) 3108-3116.
[7] S.V. Kuppu, M. Sonaimuthu, S. Marimuthu, S. Venkatesan, B. Murugesan, N. Ahmed, A. Karuppanan, P. Sengodu, A.R. Jeyaraman, S. Thambusamy, Y.R. Lee, NiO@ZnO composite bimetallic nanocrystalline decorated TiO_2-$CsPbI_3$ photo-anode surface modifications for perovskite-sensitized solar cell applications, Journal of Molecular Structure 1276 (2023) 134763.
[8] F. Du, X. Zuo, Q. Yang, B. Yang, G. Li, H. Tang, H. Zhang, M. Wu, Y. Ma, The stabilization of $NiCo_2O_4$ nanobelts used for catalyzing triiodides in dye-sensitized solar cells by the presence of RGO sheets, Solar Energy Materials and Solar Cells 149 (2016) 9-14.
[9] F. Han, S. Yun, J. Shi, Y. Zhang, Y. Si, C. Wang, N. Zafar, J. Li, X. Qiao, Efficient dual-function catalysts for triiodide reduction reaction and hydrogen evolution reaction using unique 3D network aloe waste-derived carbon-supported molybdenum-based bimetallic oxide nanohybrids, Applied Catalysis B: Environmental 273 (2020) 119004.
[10] R.A.J.J.S.R. Deshpande, Advances in Solar Cell Technology: An Overview, Journal of Scientific Research 65(02) (2021) 72-75.
[11] P. Roy, A. Ghosh, F. Barclay, A. Khare, E. Cuce, Perovskite Solar Cells: A Review of the Recent Advances, Coatings 12(8) (2022) 1089.
[12] H.F. Ummah, R. Setiati, Y.B.V. Dadi, M.N. Ariq, M.T. Malinda, Solar energy as natural resource utilization in urban areas: Solar energy efficiency literature review, IOP Conference Series: Earth and Environmental Science 780(1) (2021) 012007.
[13] K.J.P.i.P.R. Zweibel, Applications, Thin films: past, present, future, Progress in Photovoltaics: Research and Applications 3(5) (1995) 279-293.
[14] A. Goetzberger, C. Hebling, H.-W. Schock, Photovoltaic materials, history, status and outlook, Materials Science and Engineering: R: Reports 40(1) (2003) 1-46.
[15] T. Markvart, L. Castañer, Principles of solar cell operation, McEvoy's Handbook of Photovoltaics, Elsevier,The Netherlands, 2018, pp. 3-28.
[16] E.L. Meyer, E.E. van Dyk, Characterization of degradation in thin-film photovoltaic module performance parameters, Renewable Energy 28(9) (2003) 1455-1469.
[17] A.M. Adeyinka, O.V. Mbelu, Y.B. Adediji, D.I. Yahya, A review of current trends in thin film solar cell technologies, International Journal of Energy and Power Engineering 17(1) (2023) 1-10.
[18] W.M. Salih, A.M. Rheima, H.A. Kadhum, Synthesis and Characterization of) CeO (x-) CuO (1-x Nanocomposite by Simple Aqueous Route for Solar Cell Application, Research Square (2021).
[19] R. Lin, H. Lei, D. Ruan, K. Jiang, X. Yu, Z. Wang, W. Mai, H. Yan, Solar-powered overall water splitting system combing metal-organic frameworks derived bimetallic nanohybrids based electrocatalysts and one organic solar cell, Nano Energy 56 (2019) 82-91.
[20] S. Bouazizi, W. Tlili, A. Bouich, B.M. Soucase, A. Omri, Design and efficiency enhancement of FTO/PC60BM/CsSn0.5Ge0.5I3/Spiro-OMeTAD/Au perovskite solar cell utilizing SCAPS-1D Simulator, Materials Research Express 9(9) (2022) 096402.
[21] J.N. Ike, M.W. Dlamini, R.P. Dwivedi, Y. Zhang, G.T. Mola, Plasmon assisted optical absorption and reduced charge recombination for improved device performance in polymer solar cell, Journal of Physics and Chemistry of Solids 165 (2022) 110662.

[22] N. Zhang, C. Han, X. Fu, Y.-J. Xu, Function-Oriented Engineering of Metal-Based Nanohybrids for Photoredox Catalysis: Exerting Plasmonic Effect and Beyond, Chem 4(8) (2018) 1832-1861.
[23] A.Y. Ahmed, J.N. Ike, M.S. Hamed, G.T.J.J.o.A.P.S. Mola, Silver decorated magnesium doped photoactive layer for improved collection of photo-generated current in polymer solar cell, Journal of Applied Polymer Science 140(14) (2023) e53697.
[24] T. Soga, Fundamentals of solar cell, Nanostructured Materials for Solar Energy Conversion, Elsevier 2006, pp. 3-43.
[25] A.S. Al-Ezzi, M.N.M. Ansari, Photovoltaic Solar Cells: A Review, Applied System Innovation 5(4) (2022) 67.
[26] R.P. Smith, A.A.-C. Hwang, T. Beetz, E. Helgren, Introduction to semiconductor processing: Fabrication and characterization of p-n junction silicon solar cells, American Journal of Physics 86(10) (2018) 740-746.
[27] C. Zhang, High Efficiency GaAs-based Solar Cells Simulation and Fabrication, Arizona State University 2014.
[28] F. Wang, X.-K. Liu, F. Gao, Chapter 1 - Fundamentals of Solar Cells and Light-Emitting Diodes, in: F. Gao (Ed.), Advanced Nanomaterials for Solar Cells and Light Emitting Diodes, Elsevier 2019, pp. 1-35.
[29] A. Yousef, R.M. Brooks, M.H. El-Newehy, S.S. Al-Deyab, H.Y. Kim, Electrospun Co-TiC nanoparticles embedded on carbon nanofibers: Active and chemically stable counter electrode for methanol fuel cells and dye-sensitized solar cells, International Journal of Hydrogen Energy 42(15) (2017) 10407-10415.
[30] S. Visnupriya, N. Prabavathi, P. Vijayakumar, N. Santhosh, K. Pradeeswari, Bimetallic-reduced graphene oxide nanocomposites as a reactive counter electrodes for dye sensitized solar cells, Journal of Materials Science: Materials in Electronics 33(8) (2022) 5613-5625.
[31] C. Siu, Semiconductor Physics, Electronic Devices, Circuits, and Applications, Springer, Cham, Switzerland, 2022, pp. 35-39.
[32] R.K. Willardson, A.C. Beer, Semiconductors and Semimetals, Volume 12, Academic Press, London, England, UK, 1977.
[33] A.M. Imran, A. Naushad, Applications of Solar Cells, Fundamentals of Solar Cell Design, John Wiley & Sons, Ltd, Chichester, England, UK, 2021, pp. 345-369.
[34] K.H. Raut, H.N. Chopde, D.W. Deshmukh, A review on comparative studies of diverse generation in solar cell, International Journal of Electrical Engineering and Ethics 1(3) (2018) 1-9.
[35] N. Roslan, M.E. Ya'acob, D. Jamaludin, Y. Hashimoto, M.H. Othman, A.N. Iskandar, M.R. Ariffin, M.H. Ibrahim, J. Mailan, A.H. Jamaluddin, M.F. Mail, B.S.N. Aliah, L. Lu, Dye-Sensitized Solar Cell (DSSC): Effects on Light Quality, Microclimate, and Growth of Orthosiphon stamineus in Tropical Climatic Condition, Agronomy 11(4) (2021) 631.
[36] H.-P. Wang, J.-H. He, Toward Highly Efficient Nanostructured Solar Cells Using Concurrent Electrical and Optical Design, Advanced Energy Materials 7(23) (2017) 1602385.
[37] T. Kirchartz, U. Rau, What Makes a Good Solar Cell?, Advanced Energy Materials 8(28) (2018) 1703385.
[38] M.A. Green, Tracking solar cell conversion efficiency, Nature Reviews Physics 2(4) (2020) 172-173.
[39] K. Zhou, K. Xian, L. Ye, Morphology control in high-efficiency all-polymer solar cells, InfoMat 4(4) (2022) e12270.
[40] G.R. Neupane, A. Kaphle, P. Hari, Microwave-assisted Fe-doped ZnO nanoparticles for enhancement of silicon solar cell efficiency, Solar Energy Materials and Solar Cells 201 (2019) 110073.
[41] Y. Li, H. Xie, E.L. Lim, A. Hagfeldt, D. Bi, Recent Progress of Critical Interface Engineering for Highly Efficient and Stable Perovskite Solar Cells, Advanced Energy Materials 12(5) (2022) 2102730.
[42] W. Yu, X. Sun, M. Xiao, T. Hou, X. Liu, B. Zheng, H. Yu, M. Zhang, Y. Huang, X. Hao, Recent advances on interface engineering of perovskite solar cells, Nano Research 15(1) (2022) 85-103.
[43] H. Bi, G. Han, M. Guo, C. Ding, S. Hayase, H. Zou, Q. Shen, Y. Guo, W. Hou, Top-Contacts-Interface Engineering for High-Performance Perovskite Solar Cell With Reducing Lead Leakage, Solar RRL 6(9) (2022) 2200352.
[44] M. Ashraf, N.H. Hemasiri, S. Kazim, N. Ullah, M. Khan, S. Adewale Ganiyu, K. R. Alhooshani, M.N. Tahir, S. Ahmad, Interface engineering of a hole-transport layer/perovskite with low-band-gap 2D-carbon nitrides for solar cell fabrication, Sustainable Energy & Fuels 7(3) (2023) 763-768.
[45] G.-W. Kim, J. Min, T. Park, A. Petrozza, Defect Passivation through (α-Methylguanido)acetic Acid in Perovskite Solar Cell for High Operational Stability, ACS Applied Materials & Interfaces 14(18) (2022) 20848-20855.
[46] Y. Liu, W. Xiang, S. Mou, H. Zhang, S. Liu, Synergetic surface defect passivation towards efficient and stable inorganic perovskite solar cells, Chemical Engineering Journal 447 (2022) 137515.
[47] V.S. Katta, M. Velpandian, S. Challapalli, P. Meduri, S.S.K. Raavi, Defect engineered (Er3+/Nd3+) codoped TiO_2 photoanodes for enhanced photoelectrochemical and photovoltaic applications, Sustainable Energy & Fuels 6(24) (2022) 5539-5556.
[48] F.E. Subhan, A.D. Khan, F.E. Hilal, A.D. Khan, S.D. Khan, R. Ullah, M. Imran, M. Noman, Efficient broadband light absorption in thin-film a-Si solar cell based on double sided hybrid bi-metallic nanogratings, RSC Advances 10(20) (2020) 11836-11842.
[49] P.N. Kumar, A. Das, M. Deepa, P. Ghosal, A.K. Srivastava, Bimetallic Au-Ag Alloy Nanoparticles Improve Energy Harvesting of a TiO_2/CdS Film, ChemistrySelect 1(16) (2016) 5320-5330.
[50] N. Kaur, V. Bhullar, D.P. Singh, A. Mahajan, Bimetallic Implanted Plasmonic Photoanodes for TiO_2 Sensitized Third Generation Solar Cells, Scientific Reports 10(1) (2020) 7657.
[51] G.T. Mola, E.A.A. Arbab, Bimetallic nanocomposite as hole transport co-buffer layer in organic solar cell, Applied Physics A 123(12) (2017) 772.
[52] V.-D. Dao, Y. Choi, K. Yong, L.L. Larina, O. Shevaleevskiy, H.-S. Choi, A facile synthesis of bimetallic AuPt nanoparticles as a new transparent counter electrode for quantum-dot-sensitized solar cells, Journal of Power Sources 274 (2015) 831-838.
[53] M. Sharma, P.R. Pudasaini, F. Ruiz-Zepeda, E. Vinogradova, A.A. Ayon, Plasmonic Effects of Au/Ag Bimetallic Multispiked Nanoparticles for Photovoltaic Applications, ACS Applied Materials & Interfaces 6(17) (2014) 15472-15479.
[54] H.F. Zarick, W.R. Erwin, A. Boulesbaa, O.K. Hurd, J.A. Webb, A.A. Puretzky, D.B. Geohegan, R. Bardhan, Improving Light Harvesting in Dye-Sensitized Solar Cells Using Hybrid Bimetallic Nanostructures, ACS Photonics 3(3) (2016) 385-394.
[55] Y. Thaver, S.O. Oseni, G. Tessema Mola, Silver doped nickel oxide nanocomposite and photon harvesting enhancement in bulkheterojunction organic solar cell, Solar Energy 214 (2021) 11-18.
[56] F. Hazeghi, S. Mozaffari, S.M.B. Ghorashi, Metal organic framework–derived core-shell CuO@NiO nanospheres as hole transport material in perovskite solar cell, Journal of Solid State Electrochemistry 24(6) (2020) 1427-1438.
[57] Y. Zhang, S. Yun, X. Qiao, M. Sun, J. Dang, C. Dang, J. Yang, Hybridization of Mn/Ta bimetallic oxide and mesh-like porous bio-carbon for boosting copper reduction for D35/Y123-sensitized solar cells and hydrogen evolution, Journal of Alloys and Compounds 893 (2022) 162349.
[58] S.a. Liu, W. Qi, Y. Cao, C. Liang, S. Geng, H. Guo, Y. Liu, Y. Luo, W. Zhang, L. Li, Design and characterization of frog egg shaped $CoFe_2O_4$@C core-shell composite as a novel multi-functional counter electrode for low-cost energy devices, Journal of Alloys and Compounds 915 (2022) 165395.
[59] Y. Di, Z. Xiao, Z. Zhao, G. Ru, B. Chen, J. Feng, Bimetallic NiCoP nanoparticles incorporating with carbon nanotubes as efficient and durable electrode materials for dye sensitized solar cells, Journal of Alloys and Compounds 788 (2019) 198-205.
[60] L. Su, H. Li, Y. Xiao, G. Han, M. Zhu, Synthesis of ternary nickel cobalt phosphide nanowires through phosphorization for use in platinum-free dye-sensitized solar cells, Journal of Alloys and Compounds 771 (2019) 117-123.
[61] Y. Du, G. Yue, Z. Lan, Y. Gao, J. Wu, F. Tan, A dye-sensitized solar cell based on magnetic CoP@FeP4@Carbon composite counter electrode generated an efficiency of 9.88%, Inorganic Chemistry Frontiers 8(23) (2021) 5034-5044.
[62] X.-M. Lin, J.-H. Chen, J.-J. Fan, Y. Ma, P. Radjenovic, Q.-C. Xu, L. Huang, S. Passerini, Z.-Q. Tian, J.-F. Li, Synthesis and Operando Sodiation Mechanistic Study of Nitrogen-Doped Porous Carbon Coated Bimetallic Sulfide Hollow Nanocubes as Advanced Sodium Ion Battery Anode, 9(40) (2019) 1902312.
[63] X. Qian, W. Wu, J. Zhuang, Y. Niu, J. Huang, L. Hou, CoMoSx@Ni-CoMoSx double-shelled cage-in-cage hollow polyhedron as enhanced Pt-free catalytic material for high-efficiency dye-sensitized solar cell, Journal of Power Sources 417 (2019) 21-28.
[64] L.J. Ma, J.B. Shi, G. Wang, Z.Z. Fu, Y.H. Wu, B.X. Lei, Z.F. Sun, Economically synthesized $NiCo_2S_4/TiO_2$ with high reflectance ability as the counter electrode to replace Pt for dye-sensitized solar cells, Advanced Powder Technology 32(7) (2021) 2654-2661.
[65] D. Tang, R. Zhao, J. Xie, K. Zhou, Y. Han, X. Wu, H. Wu, G. Diao, M. Chen, Bimetallic sulfide Co_8FeS_8/N–C dodecahedral nanocages via cation exchange as counter electrode for dye-sensitized solar cells, Journal of Alloys and Compounds 829 (2020) 154526.
[66] Q. Wu, R. Chen, P. Su, D. Shi, Y. Zhang, K. Chen, H. Li, Co_9S_8/NC@$FeCoS_2$/NC composites with hollow yolk shell structure as the counter electrode for Pt-free dye-sensitized solar cells, Electrochimica Acta 438 (2023) 141587.
[67] N. Huang, S. Zhang, H. Huang, J. Liu, Y. Sun, P. Sun, C. Bao, L. Zheng, X.

Sun, X. Zhao, Pt-sputtering-like $NiCo_2S_4$ counter electrode for efficient dye-sensitized solar cells, Electrochimica Acta 192 (2016) 521-528.
[68] V. Arunprasad, P. Siva Karthik, S. Thulasi, G.P. Arul, M. Shkir, A.T. Rajamanickam, T. Sumathi, S.R. Fredrick, Hydrothermal Preparation of Ni_3S_4/CoS_2 Composite Electrocatalytic Materials for High Performance Counter Electrodes of Dye-Sensitized Solar Cells, Journal of Cluster Science 33(6) (2022) 2651-2659.
[69] N. Huang, R. Peng, Y. Ding, S. Yan, G. Li, P. Sun, X. Sun, X. Liu, H. Yu, Facile chemical-vapour-deposition synthesis of vertically aligned co-doped MoS_2 nanosheets as an efficient catalyst for triiodide reduction and hydrogen evolution reaction, Journal of Catalysis 373 (2019) 250-259.
[70] J. Deng, M. Wang, X. Song, Z. Yang, Z. Yuan, Ti Porous Film-Supported $NiCo_2S_4$ Nanotubes Counter Electrode for Quantum-Dot-Sensitized Solar Cells, Nanomaterials 8(4) (2018) 251.
[71] F. Li, J. Wang, L. Zheng, Y. Zhao, N. Huang, P. Sun, L. Fang, L. Wang, X. Sun, In situ preparation of NiS_2/CoS_2 composite electrocatalytic materials on conductive glass substrates with electronic modulation for high-performance counter electrodes of dye-sensitized solar cells, Journal of Power Sources 384 (2018) 1-9.
[72] K. Ramasamy, B. Tien, P.S. Archana, A. Gupta, Copper antimony sulfide (CuSbS2) mesocrystals: A potential counter electrode material for dye-sensitized solar cells, Materials Letters 124 (2014) 227-230.
[73] S. Sarihi, S. Padervand, S.M. Mousavi khoei, N. Shakiba, The effect of nitrogen concentration on N-doped diamond-like carbon films prepared by plasma-electrolytic method, Inorganic and Nano-Metal Chemistry 51(12) (2021) 1686-1696.
[74] A. Abdelaal, F. Banei, A. Fenti, M. Nili Ahmadababdi, M. Martín-Sómer, State of the art review of photocatalytic water treatment, Journal of Composites and Compounds 5(14) (2023) 51-63.
[75] S. Mirzazadeh Khomambazari, P. Lokhande, S. Padervand, N.D. Zaulkiflee, M. Irandoost, S. Dubal, H. Sharifan, A review of recent progresses on nickel oxide/carbonous material composites as supercapacitor electrodes, Journal of Composites and Compounds 4(13) (2022) 195-208.
[76] X. Liu, H. Jang, P. Li, J. Wang, Q. Qin, M.G. Kim, G. Li, J. Cho, Antimony-Based Composites Loaded on Phosphorus-Doped Carbon for Boosting Faradaic Efficiency of the Electrochemical Nitrogen Reduction Reaction, 58(38) (2019) 13329-13334.
[77] A. Arshad, S. Yun, J. Shi, M. Sun, N. Zafar, A. Hagfeldt, N-coordinated bimetallic defect-rich nanocarbons as highly efficient electrocatalysts in advanced energy conversion applications, Chemical Engineering Journal 435 (2022) 134913.
[78] A. Yousef, M.S. Akhtar, N.A.M. Barakat, M. Motlak, O.B. Yang, H.Y. Kim, Effective NiCu NPs-doped carbon nanofibers as counter electrodes for dye-sensitized solar cells, Electrochimica Acta 102 (2013) 142-148.
[79] W. Lu, R. Jiang, X. Yin, L. Wang, Porous N-doped-carbon coated $CoSe_2$ anchored on carbon cloth as 3D photocathode for dye-sensitized solar cell with efficiency and stability outperforming Pt, Nano Research 12(1) (2019) 159-163.
[80] T. Ahamad, $CoSe_2$@N-Doped Graphene Nanocomposite High-Efficiency Counter Electrode for Dye-Sensitized Solar Cells, Journal of Inorganic and Organometallic Polymers and Materials 32(7) (2022) 2568-2577.
[81] S. Ghasemi, S.R. Hosseini, Z. Kazemi, Electrochemical deposition of Pt-Ni on reduced graphene oxide as counter electrode material for dye-sensitized solar cell, Journal of Photochemistry and Photobiology A: Chemistry 348 (2017) 263-268.
[82] S.N. Ngwenya, Application of N-doped TiO_2/Bi_2O_3/rGO nanocomposites as a photoanode material in dye-sensitized solar cells, University of KwaZulu-Natal 2021.
[83] T. Raj kumar, M. Shaheer Akhtar, G. Gnana kumar, Ni–Co bimetallic nanoparticles anchored reduced graphene oxide as an efficient counter electrode for the application of dye sensitized solar cells, Journal of Materials Science: Materials in Electronics 28(1) (2017) 823-831.
[84] M. Rameez, K. Saranya, A. Subramania, N. Sivasankar, S. Mallick, Bimetal (Ni–Co) nanoparticles-incorporated electrospun carbon nanofibers as an alternative counter electrode for dye-sensitized solar cells, Applied Physics A 122(2) (2016) 71-10.
[85] N.A.M. Barakat, M. Shaheer Akhtar, I.M.A. Mohamed, Y.A. Dakka, R. Hamdan, A.G. El-Deen, K. Elsaid, M. Obaid, S. Al-Meer, Effective and stable FeNi@N-doped graphene counter electrode for enhanced performance dye sensitized solar cells, Materials Letters 191 (2017) 80-84.